J Fluoresc (2011) 21:1921–1931
DOI 10.1007/s10895-011-0891-6

ORIGINAL PAPER

A Multifunctional Fluorescence Probe for the Detection of Cations in Aqueous Solution: the Versatility of Probes Based on Peptides

Bin Wang · Hong-Wei Li · Yang Gao · Houyu Zhang · Yuqing Wu

Received: 16 January 2011 / Accepted: 2 May 2011 / Published online: 11 May 2011

Abstract We synthesized a tetra-functional fluorescence probe based on dansyl and peptide motif, dansyl-Gly-Trp (DGT, **1**), that efficiently bound several metal ions and showed distinguishing optical properties. The probe **1** could respond to Hg^{2+} with enhanced and blue-shifted fluorescence emission but to Cu^{2+} with obvious fluorescence quenching. In addition, **1** was sensitive to pH ranging from 2.0 to 5.0 and precipitated in the presence of Pb^{2+} at neutral conditions. The combination of these intrinsic properties with the selective responses to different chemical inputs allows this system to be implemented as an ionic switch. Furthermore, **1** could penetrate the cell membrane and accumulated well in intracellular region. The underlying mechanisms of the probe to different kind of metal ion were explored successfully by using either ^1H NMR, NOESY, electron paramagnetic resonance (EPR) or FT-IR spectra. In addition, to investigate the binding model of **1**/Hg^{2+} and **1**/Cu^{2+}, simulations were also performed by using density functional theory (DFT) and reasonable binding configurations were achieved for these two complexes.

Keywords Peptide · Fluorescence probe · Multifunction · Mercury · Copper

Electronic supplementary material The online version of this article (doi:10.1007/s10895-011-0891-6) contains supplementary material, which is available to authorized users.

B. Wang · H.-W. Li · Y. Gao · H. Zhang · Y. Wu (✉)
State Key Laboratory of Supramolecular Structure and Materials, Jilin University,
No. 2699, Qianjin Street,
Changchun 130012, China
e-mail: yqwu@jlu.edu.cn

Introduction

The design and synthesis of optical probes with high selectivity and sensitivity to heavy transition-metal ions (HTMs), particularly mercury, lead, and copper ions, have attracted special attention due to the toxicity of these ions, both in physiological systems and in the environment. In numerous successful applications, the design of probes, has been essentially based on structure-activity relationship [1–3]. However, most probe designs were based on the assumption that one probe would bind to one target. Thus, the majority of probes have been restricted to measuring the concentration of one specific target ion. However, quite often, the contamination of physiological and/or environmental conditions results from the synergistic contribution of two or more infectants. Therefore, it would be beneficial to develop probes with multifunctional capabilities that could identify two or more infectants in a system. Moreover, it would be very useful, both in chemistry and material sciences, to develop fluorescence probes for metal ions that could be integrated into molecular level devices, like logic gates and/or ionic switches [4–7].

In the previous studies, the concept that introducing amino acids as binding site of probe have been proved successful [8–10]. Highly sensitive fluorescence probes derived from pyrene butyric acid for Pb^{2+} [8] and dansyl moiety for Hg^{2+} [9, 10] have been achieved, which displayed rapid and specific optical responses to target metal ion in buffered aqueous solution. In the present study, instead of using single amino acid, the motif of peptide will be introduced to design fluorescence probe for metal ions. By tuning the number and sequence of participant amino acids several attractive features of probe will be achieved as: (i) felicitous hydrophilicity and hydrophobicity, in keeping the balance between water-solubitily and cell

permeability; (ii) easily optimized high selectivity and sensitivity to different metal ions; and essentially (iii) possessing more binding site in comparison to a single amino acid, which supply a possibility to be used as a logic gate or molecular switch to different kinds of metal ions. Although some probes based on peptide motif had been developed for metal ions [11–14], they could not response to different metal ions simultaneously. In the present study, two dansyl labeled peptides, dansly-Gly-Trp (DGT, **1**) and dansly-Gly-Gly-Trp (DGGT, **2**) (Fig. 1) were synthesized, in possessing of multiple binding sites that would confer the potential to be used as a logic gate or molecular switch for different kinds of metal ions.

Experimental

Materials and Apparatus

All chemicals were obtained from commercial suppliers and used without further purification. Mass spectra were measured on a QTRAP mass spectrometer (Applied Biosystems Sciex Foster city, USA). Infrared (IR) spectra were recorded on a Bruker Vertex 80 V FTIR spectrophotometer.

General Method

Fluorescence emission spectra were recorded on a Shimadzu (Japan) RF-5301PC fluorescence spectrophotometer. To reduce the fluctuation in the excitation intensity during measurement, the lamp was kept on for 1 h and the samples were stock-still for 3 min prior to the experiment. Samples for emission measurement were placed in a 1 cm× 1 cm quartz cuvettes (4 mL volume). All spectroscopic measurements of **1** and **2** were performed in 10.0 mM HEPES buffer solution (pH 7.4), and the concentrations of **1** and **2** in all the fluorescent experiments are 20.0 μM. A fixed excitation wavelength at 330 nm was used. Fluorescence titration was performed in buffer solution using respective chloride salt of metal ions except for $AgNO_3$.

UV–vis absorption spectra were recorded on a Shimadzu (Japan) UV-3100 spectrophotometer. To reduce the fluctuation of baseline in absorbance spectra, the lamp was kept on for 0.5 h before the measurement. Sample for measurement was placed in a 1 cm×1 cm quartz cuvette (4 mL volume). The absorption spectra of **1** (20.0 μM) were measured in 10.0 mM HEPES buffer solution (pH 7.4).

Turbidity measurements of **1** were recorded on an Ocean Optic usb-4000 spectrophotometer upon addition of Pb^{2+}. The lamp was kept on for 0.5 h before measurements. Sample for test was placed in a 1 cm×1 cm cuvette (4 mL volume). The absorption spectra of **1** (20 μM) with addition of Pb^{2+} were recorded in 10.0 mM HEPES buffer solution (pH 7.4) with stirring.

^1H NMR titration experiments were conducted on a Bruker Varian Unity-500 MHz spectrometer. We carried out ^1H NMR titration experiments on a 5×10^{-4} M solution of **1** in D_2O containing 0.3% (*v*/*v*) d_6-DMSO. The spectra were recorded in the presence of 0.5 and 1 equiv. Hg^{2+}, respectively at room temperature. The NOESY experiment was performed at 25 °C in the presence of **1** equiv. Hg^{2+}.

The EPR spectra were recorded on a JES-FA 200 EPR spectrometer. The instrumental parameters were as follows: scanning frequency, 9.45 GHz; central field, 3301.85 G; scanning width, 8,000 G; scanning power, 0.998 mW; scanning temperature, 25 °C. 2,2-Diphenyl-1-picrylhydrazyl (DPPH) was used as a reference for the calculation of spin concentration. The precipitate for EPR test was obtained from the solution of **1** and equivalent $CuCl_2$.

Density functional theory simulations were performed with the B3LYP functional and the mixed "Double-ζ" quality basis sets 6–31 G(d) for C, H, O, N, S and

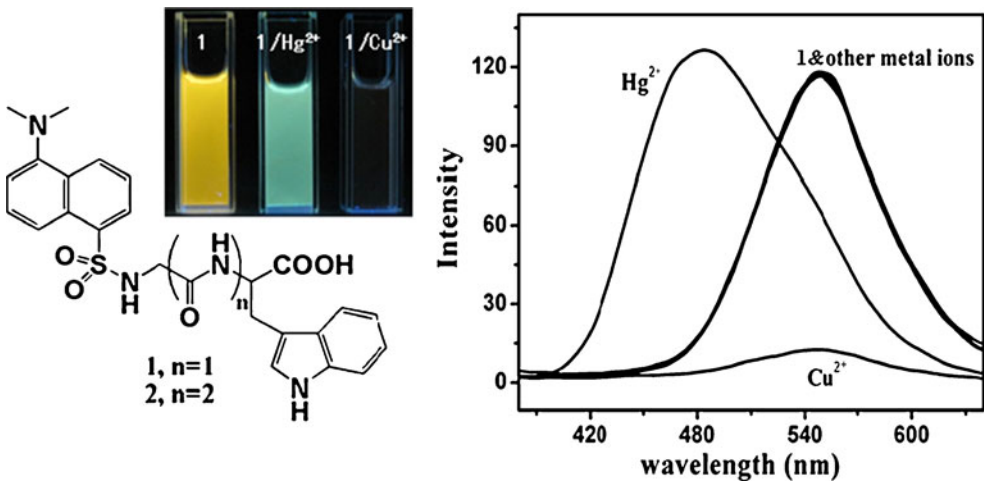

Fig. 1 Tetra-functional probes (**1** and **2**) based on a dansyl moiety and a peptide motif. (*Left*) Chemical structure of **1** and **2**; (*middle*) fluorescence images of **1**, **1**/Hg^{2+}, and **1**/Cu^{2+}; (*right*) fluorescence spectra of 20 μM **1** in 10 mM HEPES solution (pH 7.4) in the presence of 40 μM Hg^{2+}, 80 μM Cu^{2+}, and 100 μM of other metal ions (K^+, Na^+, Mg^{2+}, Al^{3+}, Zn^{2+}, Fe^{3+}, Mn^{2+}, Co^{2+}, Cd^{2+}, Ca^{2+}, Ag^{2+}, Ni^{2+}) (λ_{ex}= *330 nm)*

LANL2DZ for Hg and Cu. Optimization of the complexes was performed without any constraints for all the complexes. All calculations were carried out using Gaussian 09 [15].

Cell Permeability

Cells Culture

HEK-293 cells were cultured according to the reported protocol [16]. Briefly, cells were cultured at 37 °C in Dulbecco's modified Eagle's medium (DMEM, Sigima) containing 10% fetal bovine serum (FBS, Gibco) in a 5% CO_2/95% air incubator. Cells were plated 24 h before study into 6 well plates and at the time of study, the medium was changed with a fresh 2% serum one.

Fluorescence Imaging Measurements of Probe in Cells

Imaging experiments were performed with a FV1000 confocal laser-scanning fluorescent microscope (Olympus, Japan) with a 20× objective lens. Excitation of **1** and **2**-loaded cells at 405 nm were carried out with an argon-ion laser, and emission was collected in a window from 480 to 580 nm. **1** or **2** (from a 1.0 mM stock solution in DMSO) was added to each well except the control of cultured cells and a 20 μM of **1** or **2** was obtained in final. The cells were incubated with **1** or **2** for 1 h at 37 °C, and then the medium was removed and the cells were washed thoroughly twice by PBS (pH 7.0). After that, the fluorescence microscopic image was recorded for each case.

General Procedure for the Synthesis of 1 and 2

Phthalimidoglycine (**4**)

Firstly, the mixture of phthalic anhydride (1.63 g, 11 mM) and glycine (0.75 g, 10 mM) was fused at 140 °C for 0.5 h. And then it was cooled to room temperature and the resulted solid was recrystallized from ethanol/water solution. After filtrating, drying in vacuum, we obtained compound **4** (1.95 g, 95%) as a light yellow solid. ^{1}H NMR (500 MHz, d_6-DMSO): δ=4.32 (s, 2H, CH_2), δ=7.89–7.96 (m, 4H, Pht-H).

Methyl 2-(2-(1,3-dioxoisoindolin-2-yl)acetamido)-3-(1H-indol-3-yl) propanoate (**6**)

Thionyl chloride (1.5 equiv.) was added dropwise to the solid state of **4** (1 g, 4.87 mM), and the mixture was heated under reflux for 6 h. The excess of thionyl chloride was evaporated in vacuum, and the residue was recrystallized from n-hexane three times. The produced white solid was dissolved in CH_2Cl_2 (20 mL), and then was added dropwise to an ice-cooled mixture of L-tryptophan methyl ester (1.1 equiv.) and triethylamine (1.2 equiv.) in CH_2Cl_2 (20 mL). The mixture was stirred overnight at room temperature. After dilution with CH_2Cl_2, the mixture was washed with saturated $NaHCO_3$ aqueous solution, diluted HCl, and brine step by step. The organic phase was dried over anhydrous $MgSO_4$, filtered and evaporated under reduced pressure. The resulted residue was purified by column chromatography to produce a yellow solid **6** (1.68 g, 85%). ^{1}H NMR (500 MHz, d_6-DMSO): δ=3.05–3.19 (m, 2H, CHCH_2), δ=3.58 (s, 3H, $COOCH_3$), δ=4.24 (s, 2H, CH_2CONH), δ=4.50–4.55 (m, 1H, C*H*$COOCH_3$), δ=6.98–7.49 (m, 5H, indole-H), δ=7.87–7.93 (m, 4H, Pht-H), δ=8.76–8.77 (d, 1H, CONH), δ=10.93 (s, 1H, indole-NH).

Methyl 2-(2-aminoacetamido)-3-(1H-indol-3-yl)propanoate (**7**)

To a solution of pseudodipeptide **6** (1 g, 2.5 mM) in EtOH, hydrazine monohydrate (200 μL) was added. The mixture was stirred at room temperature for 72 h, and then it was cooled to 0 °C and phthalhydrazide was removed by filtering. The filtrate was concentrated and the resulted oil was redissolved in a minimum amount of EtOH. The solution was cooled to 0 °C, filtered and evaporated under reduced pressure. The resulted pale yellow oil **7** was immediately used for the next reaction, without further purification.

Methyl 2-(2-(5-(N,N-dimethylamino)naphthalene-1-sulfonamido)acetamido)-3-(1H-indol-3-yl)propanoate (**8**)

In an ice bath, a solution of dansyl chloride (0.62 g, 2.08 mM) in CH_2Cl_2 (20 ml) was added slowly to a mixture of **7** and triethylamine in CH_2Cl_2 (30 ml) and then was stirred for 0.5 h. The reaction was kept stirring for 12 h at room temperature, and the progress of the reaction was monitored by thin layer chromatography (TLC). After dilution with CH_2Cl_2, the mixture was washed with saturated $NaHCO_3$ aqueous solution, diluted HCl, and brine one by one. The organic phase was dried over anhydrous $MgSO_4$, filtered and evaporated under reduced pressure. The resulted residue was purified by column chromatography to produce a yellow solid **8** (0.9 g, 86%). ^{1}H NMR (500 MHz, d_6-DMSO): δ=2.81 (s, 6H, CH_3NCH_3), δ=2.90–3.05 (m, 2H, CHCH_2), δ=3.51–3.53 (m, 5H, CH_2CONH + $COOCH_3$), δ=4.39–4.43 (m, 1H, C*H*$COOCH_3$), δ=6.94–8.27 (m, 11H, dansyl-H + indole-H), δ=8.27–8.29 (d, 1H, CONH), δ=8.43–8.44 (d, 1H, SO_2NH), δ=10.87 (s, 1H, indole-NH).

2-(2-(5-(N,N-dimethylamino)naphthalene-1-sulfonamido) acetamido)-3-(1H-indol-3-yl)propanoic acid (**1**)

To a stirred solution of **8** (0.5 g) in methanol, 1 M NaOH (50 mL) was added, and the mixture was stirred overnight at room temperature. The aqueous phase was acidified to pH 5–6 by using an aqueous solution of HCl, and then extracted with EtOAc three times. The combined organic phase were washed with brine, dried over Na_2SO_4, filtered and evaporated under reduced pressure step by step. Purification of 1 was performed by using column chromatography on silica gel. Target molecule **1** was obtained as a yellow solid (0.42 g, 85%). ^{1}H NMR (500 MHz, d_6-DMSO): δ=2.81 (s, 6H, CH_3NCH_3), δ=2.90–3.10 (m, 2H, CHCH_2), δ=3.43–3.48 (m, 2H, CH_2CONH), δ=4.33–4.37 (m, 1H, C*H*COOH), δ=6.91–8.9 (m, 11H, dansyl-H + indole-H), δ=8.27–8.29 (d, 1H, CONH), δ=8.42–8.44 (d, 1H SO_2NH), δ=10.82 (s, 1H, indole-NH). ^{13}C NMR (500 MHz, d_6-DMSO): δ=28.14 (CH*C*H_2), δ=42.68 (N*C*H_3), δ=45.93 (*C*H_2CONH), δ=55.0 (*C*HCOOH), δ=110.97–152.2 (dansyl-C + indole-C), δ=167.74 (*C*H_2*C*ONH), δ=174.6 (CH*C*OOH). IR (KBr) 3,394, 2,932, 2,863, 2,834, 2,785, 1,720, 1,663, 1,615, 1,587, 1,573, 1,458, 1,410, 1,326, 1,160, 1,144, 1,098 cm^{-1}. Mass spectral data (ESI-MS): for $C_{25}H_{26}N_4SO_5$, calcd. 494.16; found 495.1.

Methyl 2-(2-(2-(1,3-dioxoisoindolin-2-yl)acetamido)acetamido)-3-(1H-indol-3-yl)propanoate (**9**)

The obtained pale yellow oil **7** was dissolved in a mixture of 1:20 (*v*/*v*) DMF and CH_2Cl_2. To the solution, 1.5 equiv. Et_3N and 1.1 equiv. **4** were added with stirring. When all the reagents dissolved, 1.5 equiv. 1-Ethyl-3-(3-dimethylaminopropyl)carbodiimide (EDC) was added, and the mixture was stirred for 5–6 h at room temperature and the progress of the reaction was monitored by TLC. After dilution with CH_2Cl_2 the mixture was washed with saturated $NaHCO_3$ aqueous solution, diluted HCl, and brine. The organic phase was dried over anhydrous $MgSO_4$, filtered and evaporated under reduced pressure. The resulted residue was recrystallized from ethanol to give a pale yellow solid **9**. ^{1}H NMR (500 MHz, d_6-DMSO): δ=3.03–3.18 (m, 2H, CHCH_2), δ=3.57 (s, 3H, $COOCH_3$), δ=3.70–3.81 (m, 2H, CONHCH_2CONH), δ=4.26 (s, 2H, CH_2CONH), δ=4.51–4.55 (m, 1H, C*H*$COOCH_3$), δ=6.97–7.45 (m, 5H, indole-H), δ=7.86–7.92 (m, 4H, Pht-H), δ=8.33–8.35 (d 1H, CON*H*CH), δ=8.48–8.50 (t, 1H, CON*H*CH_2), δ=10.86 (s, 1H, indole-NH).

The target molecule **2** and the intermediates in the synthesis route were obtained under the identical conditions as mentioned, and the corresponding assayed results by ^{1}H NMR and Mass Spectrum are described as follows:

Methyl 2-(2-(2-(5-(N,N-dimethylamino)naphthalene-1-sulfonamido)acetamido) acet-amido)-3-(1H-indol-3-yl)propanoate (**11**)

^{1}H NMR (500 MHz, d_6-DMSO): δ=2.82 (s, 6H, CH_3NCH_3), δ=3.01–3.17 (m, 2H, CHCH_2), δ=3.48 (s, 2H, SO_2NHCH_2CONH), δ=3.60–3.71 (m, 2H, CONHCH_2CONH), δ=4.49–4.53 (m, 1H, C*H*$COOCH_3$), δ=6.91–8.28 (m, 11H, dansyl-H + indole-H), δ=8.29–8.31 (m, 2H, CON*H*CH_2CON*H*), δ=8.44–8.46 (d, 1H SO_2NH), δ=10.86 (s, 1H, indole-NH).

2-(2-(2-(5-(N,N-dimethylamino)naphthalene-1-sulfonamido)acetamido) acetamido)-3-(1H-indol-3-yl) propanoic acid (**2**)

^{1}H NMR (500 MHz, d_6-DMSO): δ=2.82 (s, 6H, CH_3NCH_3), δ=2.97–3.19 (m, 2H, CHCH_2), δ=3.47 (s, 2H, SO_2NHCH_2CONH), δ=3.56–3.69 (m, 2H, CONHCH_2CONH), δ=4.33–4.41 (m, 1H, C*H*COOH), δ=6.94–8.11 (m, 11H, dansyl-H + indole-H), δ=8.27–8.31 (m, 2H, CON*H*CH_2CON*H*), δ=8.44–8.46 (d, 1H SO_2NH), δ=10.78 (s, 1H, indole-NH). ^{13}C NMR (500 MHz, d_6-DMSO): δ=28.14 (CH*C*H_2), δ=42.68 (N*C*H_3), δ=45.93 (CONH*C*H_2CONH), δ=46.11 (SO_2NH*C*H_2CONH) δ=54.40 (*C*HCOOH), δ=110.97–152.2 (dansyl-C + indole-C), δ=168.77 (CONHCH_2*C*ONH), δ=168.90 (*C*ONHCH_2CONH), δ=174.6 (CH*C*OOH). IR (KBr) 3,361, 2,974, 2,865, 2,789, 1,720, 1,660, 1,533, 1,455, 1,407, 1,348, 1,330, 1,230, 1,143 cm^{-1}. Mass spectral data (ESI-MS): for $C_{27}H_{29}N_5SO_6$, calcd. 551.18; found 552.1.

Results and Discussion

We started the synthesis with free glycine (**3**), which was firstly phthaloylated with phthalic anhydride to give N-phthalimido-protected amino acid **4** in a high yield. The resulted pure **4** was reflux in excess of thionyl chloride to give carboxyl chloride **5** which was coupled with C-protected L-tryptophan to give methyl esters **6** directly without further purification. Hydrazinolysis of the phthalimido protected **6** produced the crucial amine intermediate **7**, which was unstable to heat and prolonged storage at room temperature. Free amine **7** was immediately mixed with dansyl chloride in CH_2Cl_2 solution. The resulted compound **8** was converted by alkaline hydrolysis to the first target product, dansyl-Gly-Trp (**1**). The dansyl labeled tripeptide probe, dansyl-Gly-Gly-Trp (**2**), was obtained by using the similar method (Scheme 1). After synthesis, probe **1** and **2** were assayed with Mass, Infrared, ^{1}H NMR and ^{13}C NMR spectroscopy.

Scheme 1 Synthesis route of probes **1** and **2**

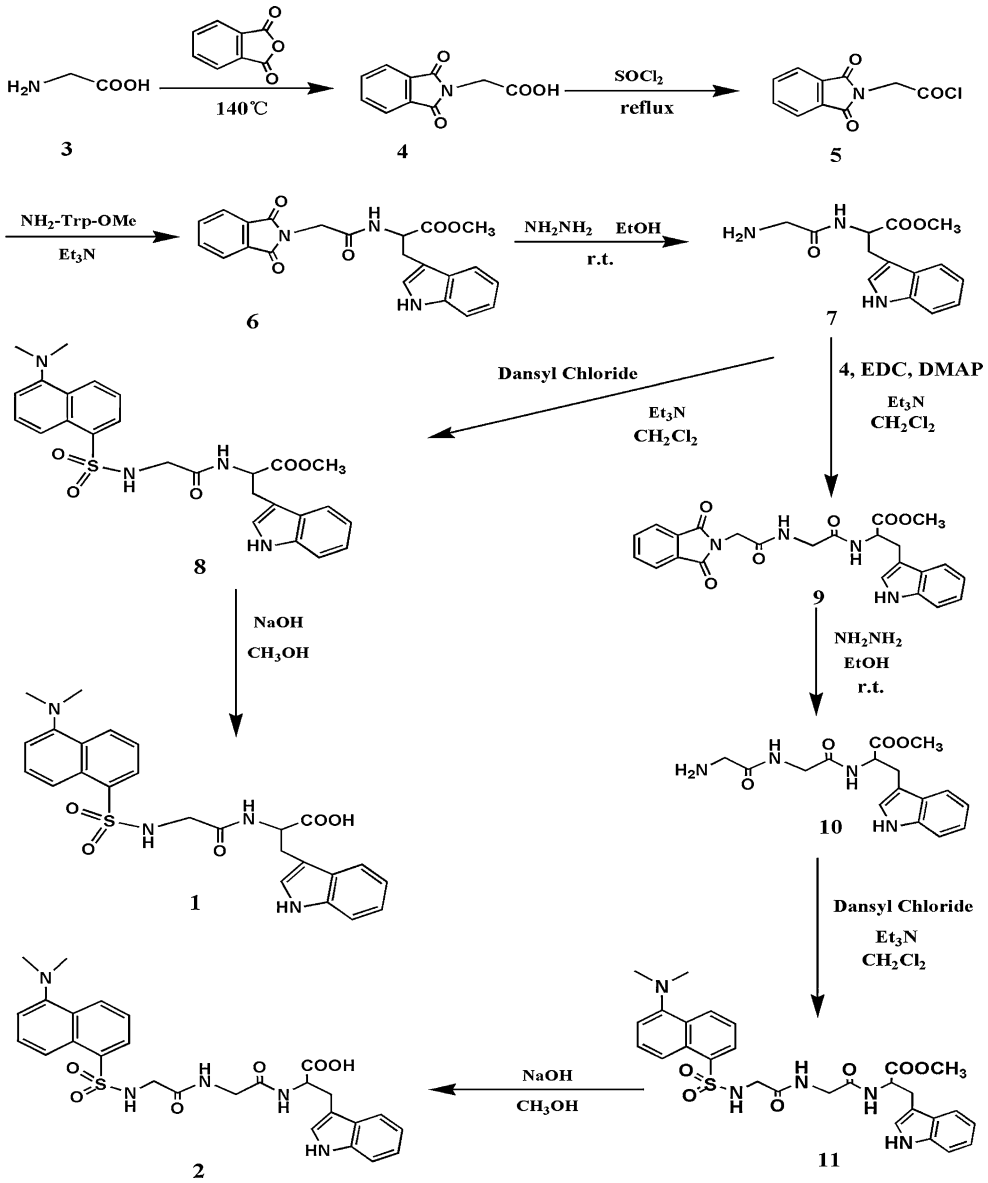

pH Effect of DGT

In solutions with pH values that ranged from 7.4 to 5.0, probe **1** did not exhibit any detectable changes in either the UV-visible absorption or the fluorescence emission spectrum. However, when the pH was lower than 5.0, with pH decrease, the intensity of a absorption band at 284 nm increased with a simultaneous decreases of the intensity of the absorption bands at 250 and 330 nm (left in Fig. 2). In addition, the corresponding fluorescence emission spectra showed unilateral quenching of a band at 550 nm (right in Fig. 2). Both results were ascribed to the protonation of the dimethylamino group in **1,** because the absorption band at 284 nm was characteristic of the protonated form of the dansyl moiety [6, 17, 11].

Absorption and Fluorescence Titration with Hg^{2+}

When Hg^{2+} (1∼80 μM) was added to **1**, we observed a significant decrease in the emission band at 550 nm and a simultaneous increase in a new band at 485 nm (left in Fig. 3). The plot of intensity ratios (I_{485}/I_{550}) to Hg^{2+} concentration (right in Fig. 3) indicates a detection limit around 5 μM of **1** to Hg^{2+}. In addition, the UV–vis absorption spectra displayed a decrease of the intensity of absorption band at 330 nm and an increase at lower wavelengths (Fig. S1†). Both changes were attributed to the formation of a **1**/Hg^{2+} complex, which reduced the ability of the sulfonamide group to donate electrons to the dansyl moiety. This inhibited the internal charge transfer between the amide group and the dansyl moiety, and

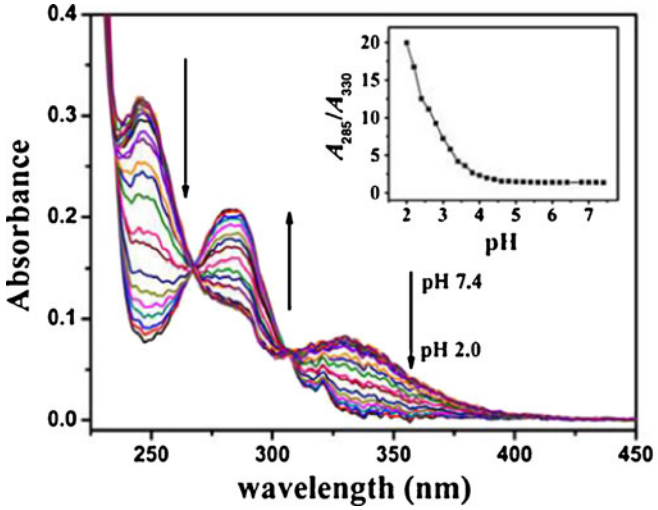

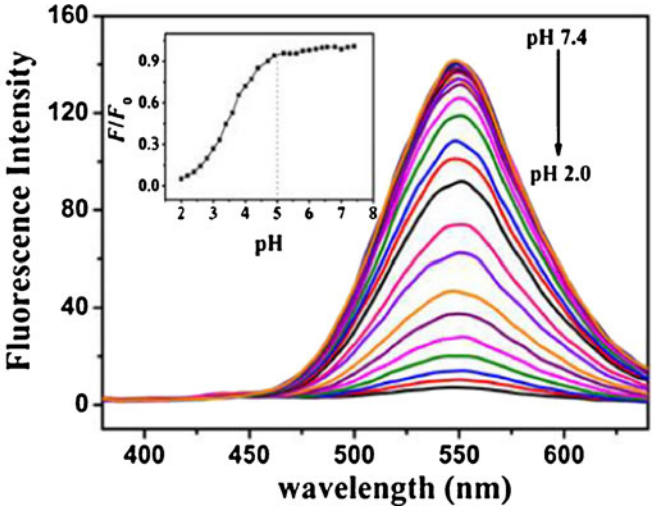

Fig. 2 (*left*): Variations of absorbance spectra of **1** (20 μM) at different pH values (2.0–7.4); *Inset*: the plot of absorbance band ratio at 285 to 330 nm (A_{285}/A_{330}) as a function of pH. (*right*): Fluorescence emission spectra of **1** (20 μM) at different pH values (2.0–7.4); The emission intensity at 550 nm quenched with pH decrease when pH is lower than 5.0 (λ_{ex}=330 nm)

consequently, both the absorption and emission bands shifted toward the blue region of the spectra. The changes in the fluorescence emission ratio of **1** with Hg^{2+} concentration were fit with the B-H plot [18]. The resulting good linear fit demonstrated that the **1**/Hg^{2+} complex formed at a 1:1 stoichiometry with a 1.18×10^3 M^{-1} binding constant (Fig. S2†). Moreover, **1** exhibited a 0.5 M fraction maximum on the Job's plot, which further confirmed a 1:1 stoichiometry for the **1**/Hg^{2+} complex (Fig. S3†).

Next, we investigated the fluorescence of **1** to Hg^{2+} in different pH conditions. Probe **1** exhibited adequate sensitivity for Hg^{2+} at pH between 6.0 and 8.0, with a maximum I_{485}/I_{550} value at pH=7.4 (Fig. S4†). This indicated that **1** was most sensitive to Hg^{2+} at physiological pH.

Binding Model of DGT/Hg^{2+}

We explored the coordination model between **1** and Hg^{2+} with both ^{1}H NMR titration (Fig. 4 and Table S1†) and 2D Nuclear Overhauser Effect Spectroscopy (NOESY) (Fig. 5). The addition of 1 equiv. of Hg^{2+} caused large chemical shifts in the H(8) (Δδ=0.08 ppm), H(5) (Δδ=0.04 ppm), H(3) (Δδ=0.1 ppm), and H(9) (Δδ=0.03 ppm) of **1**, indicating that Hg^{2+} interacted with **1** *via* the sulfonamide moiety. In addition, the chemical shifts of H

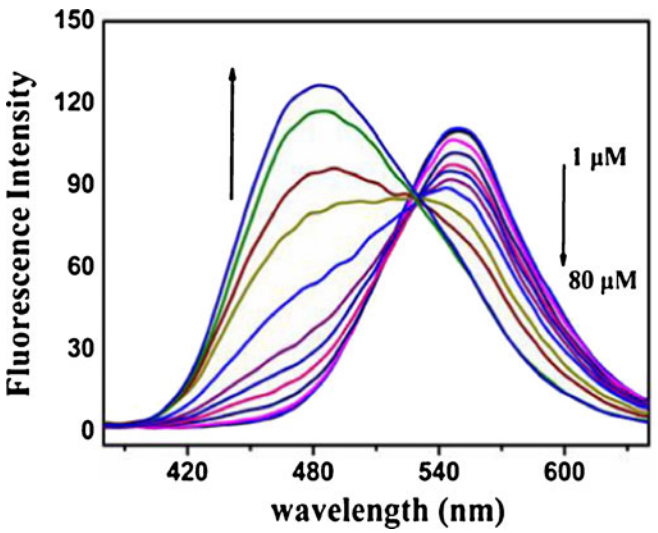

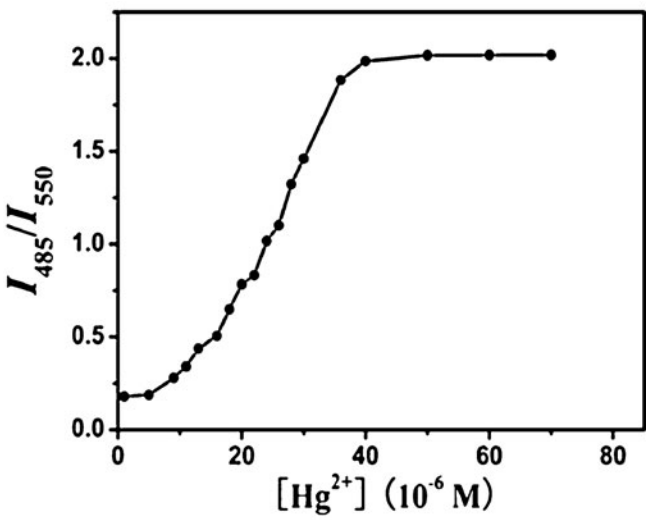

Fig. 3 Formation of a complex between probe **1** and Hg^{2+}. (*Left*) Fluorescence titration spectra of **1** (20 μM) in buffer with different concentrations of Hg^{2+}; (*right*) the corresponding plot of intensity ratios (I_{485}/I_{550}) vs. Hg^{2+} concentration (λ_{ex}=330 nm)

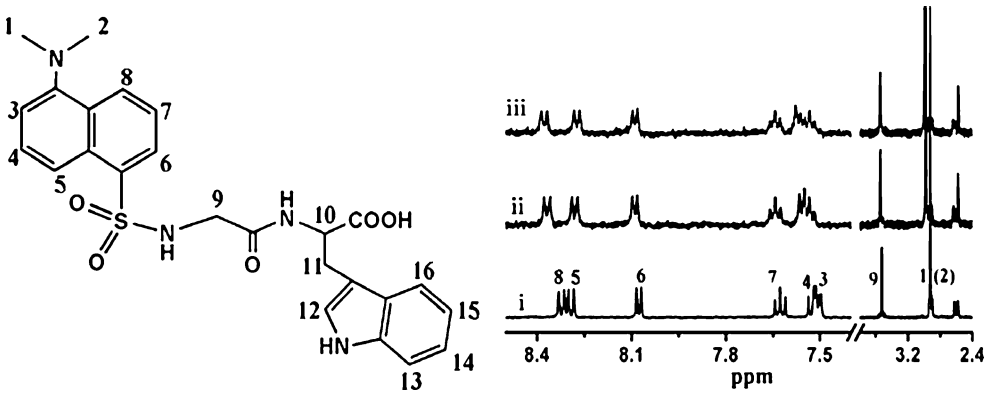

Fig. 4 Typical ^{1}H NMR spectrum of **1** (i) alone and in the presence of (ii) 0.5 and (iii) 1 equiv. of Hg^{2+} in D_2O solutions containing 0.3% DMSO-d_6

(12) ($\Delta\delta$=0.027 ppm) and H(14) ($\Delta\delta$=0.01 ppm) demonstrated that the indole ring may have a cooperative effect on Hg^{2+} complexation. In the NOESY spectrum, the strong cross peaks between H_5–H_9, H_6–H_9, H_1–H_{12}, H_1–H_{15}, and H_1–H_{16} (Fig. 5) showed that the indole ring and methylene were spatially close to naphthalene. Due to the flexibility of peptides, it is reasonable that Hg^{2+} interact with the multisites of **1** to form a stable complex. A density functional theory (DFT) simulations of possible structures provide a verification of our assumption and interpret ^{1}H correlation data well. A simulated structure with the binding configuration revealed that the sulfonamide in **1** is the primary binding sites for Hg^{2+} (left in Fig. 6).

Absorption, Fluorescence Spectrum and Binding Model of DGT/Cu^{2+}

In contrast to the changes observed with Hg^{2+}, the addition of Cu^{2+} to **1** induced a gradual fluorescence quenching. This was mainly attributed to the paramagnetic nature of Cu^{2+} and factors induced either by the formation of a **1**/Cu^{2+} complex or by the close proximity of free Cu^{2+} to the dansyl moiety [19–21]. The latter possibility of close proximity was ruled out by the changes observed in the absorption spectra of **1** after the addition of Cu^{2+} (left in Fig. 7). In particular, the large differences in the X-band electron paramagnetic resonance (EPR) spectra between $CuCl_2$ and **1**/Cu^{2+} (Fig. 8) indicated that there was a strong interaction between **1** and Cu^{2+}. The large contribution of the carboxyl in **1** to Cu^{2+} binding was confirmed by using a control compound, **8** (Fig. S5†), which had the same structure as **1** except the carboxyl was esterfied with a methyl group. Upon the addition of Cu^{2+}, **8** exhibited only very slight fluorescence quenching. Moreover, because Cu^{2+} could deprotonate the amide nitrogen when the pH>4 [19], we proposed that **1** became a loop structure after Cu^{2+} formed a complex with the sulfonamide moiety, the amide group, and the carboxylate group. DFT simulation was also conducted to optimize the configuration of **1**/Cu^{2+} (right in Fig. 6), which confirmed the proposed structure for **1**/Cu^{2+}. The fluorescence intensity ratio, F/F_0, in decreasing with Cu^{2+} concentration (inset in Fig. 7), revealed a 1 μM detection limit of **1** to Cu^{2+} in aqueous solution. This detection limit is to be satisfactory to the maximum concentration of Cu^{2+} allowed in drinking water by the U. S. EPA (~20 μM) [22]. When the S-V equation [23] was fit to the fluorescence titration data of Cu^{2+} to **1**, we found that the complex was formed at a 1:1 stoichiometry with a binding constant of 1.58×10^5 M^{-1} (Fig. S6†). The stoichiometry was further supported by the Job's plot (Fig. S7†). Of not is that the further addition of EDTA or histidine could fully snatch **1** from the **1**/Cu^{2+} complex (Fig. S8†), which

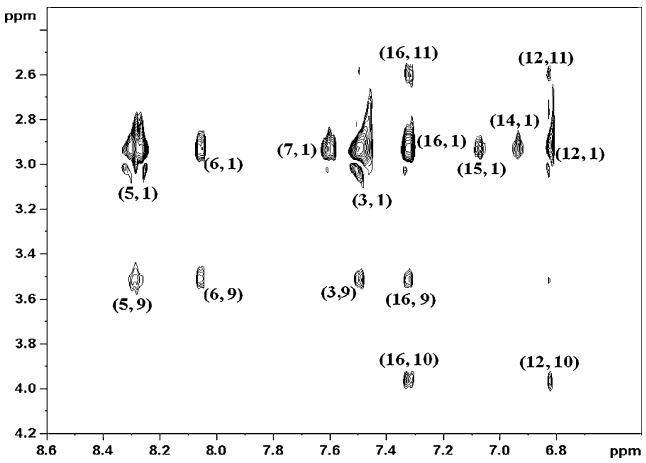

Fig. 5 The coordination between probe **1** and Hg^{2+}. Partial 500 MHz ^{1}H-^{1}H Nuclear Overhauser Effect Spectroscopy (NOESY) spectra of **1** in the presence of 1 equiv. of Hg^{2+} in D_2O solution with 0.3% DMSO-d_6

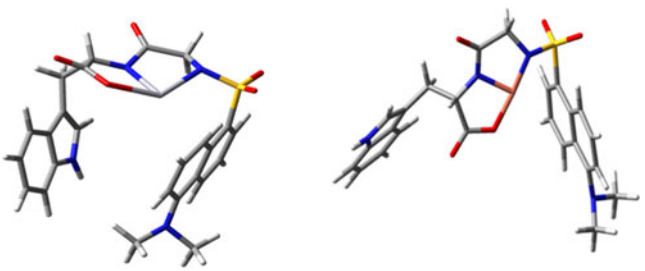

Fig. 6 The simulated structural configuration of **1**/Hg^{2+} (*left*) and **1**/Cu^{2+} (*rigth*) complexes

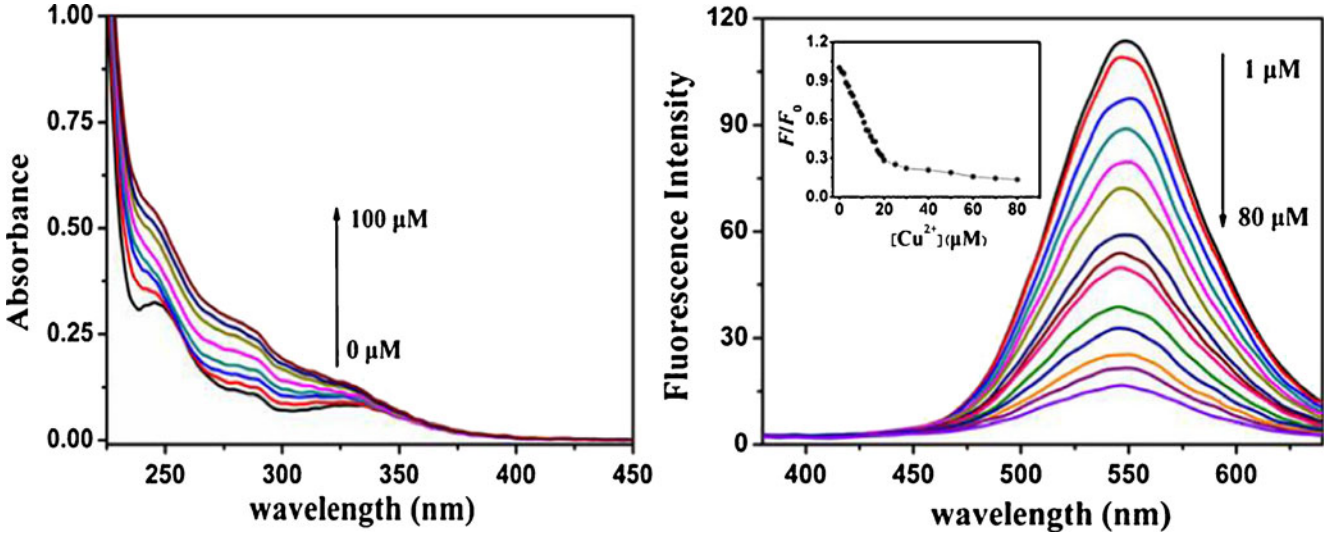

Fig. 7 (*left*) Variations of absorbance spectra of **1** (20 μM) in buffer solution upon addition of Cu^{2+} from 2.0 to 100 μM. (*right*) Fluorescence titration spectra of **1** (20 μM) in buffer solution with Cu^{2+}. The fluorescence emission intensity at 550 nm decreased upon gradually addition of Cu^{2+} from 1.0 to 80 μM (λ_{ex}=330 nm)

supply a potential application of **1**/Cu^{2+} complex in protein detection.

Design of Logic Gate

The larger binding constant of **1**/Cu^{2+} (1.58×10^5 M^{-1}) vs. that of **1**/Hg^{2+} (1.18×10^3 M^{-1}) made it possible to replace Hg^{2+} in the **1**/Hg^{2+} complex with Cu^{2+}, but not the reverse. That is, when Cu^{2+} was added to a solution that contained **1** and Hg^{2+}, we observed obvious fluorescence emission quenching (Fig. S9†). This indicated that **1** could be acted as a potential logic gate, or molecular switch, in the detection of metal ions. We utilized our system as a NOR logic gate with a YES logic function (Fig. 9). The truth table values for output 1 formed a NOR logic gate, and the truth table values for output 2 formed a YES logic gate. The combination of these intrinsic properties with the selective actions of different chemical inputs allows this system to be implemented as a complex ionic switch.

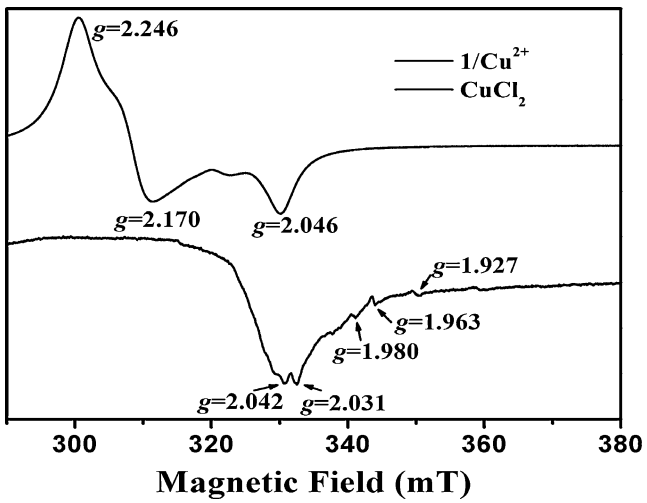

Fig. 8 Electron paramagnetic resonance (EPR) spectra indicated a strong interaction between $CuCl_2$ and probe **1**. A representative region of the X-band EPR spectra of $CuCl_2$ and its complex with 1 equiv. of **1** in the solid state. In the presence of **1**, the peaks at 300 and 325 mT disappeared, and a multitude of obvious spectral features (hyperfine splittings of the ^{14}N nuclear spins of the peptide with the unpaired electron spin of Cu^{2+}) appeared at 325–350 mT, proving that a complex formed between Cu^{2+} and **1**

Absorption Spectrum and Binding Model of DGT/Pb^{2+}

The addition of Pb^{2+} to a solution that contained **1** produced a precipitate; this was further confirmed by measuring the solution turbidity while stirring (A_{500}, Fig. S10†). The solution turbidity increased gradually with the addition of small amounts of Pb^{2+} between 3.0 and 90 μM, which indicated that an insoluble substance was generated

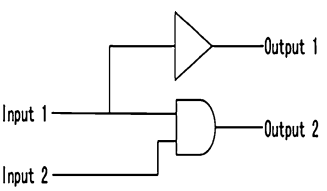

Input 1 (Hg^{2+})	Input 2 (Cu^{2+})	Output 1 (I_{485})	Output 2 (I_{550})
0	0	0	1
0	1	0	0
1	0	1	1
1	1	0	0

Fig. 9 (*left*) Combinatorial logic circuit of a dual output molecular switch; Truth table for logic gate; (*right*) Hg^{2+} and Cu^{2+} are inputs to the system; I_{485} and I_{550} are the output signals

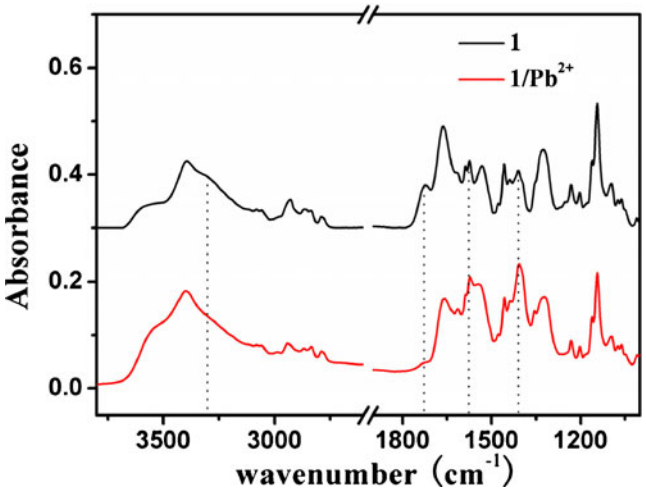

Fig. 10 Typical FT-IR spectra region of **1** in solid and that of the precipitate of **1**/Pb^{2+}

gradually. When the concentration of Pb^{2+} exceeded 120 μM, the turbidity increased dramatically to the extent that the precipitate could be observed with the naked eye. To explore the structural origin of the precipitate, it was filtrated and analyzed by using FT-IR spectroscopy and the spectra were recorded (Fig. 10). The strong peak at 1,724 cm^{-1} was assigned to a carboxyl (C=O) stretching model, which disappeared with the formation of a **1**/Pb^{2+} complex. Two strong peaks at 1,573 and 1,409 cm^{-1} were assigned to antisymmetric and symmetric C=O stretching models of the carboxylate. It is reasonable to propose that the carboxyl of **1** bound directly to Pb^{2+}, and no other functional group interacted with Pb^{2+}. Furthermore, based on previous reports [24–29], the large difference between $\nu_{COO}{}^{as-}$and $\nu_{COO}{}^{s-}$ ($\Delta\nu$=164 cm^{-1}) was ascribed to a bidentate chelation model between the carboxylate and Pb^{2+}. In addition, the response of the control compound **8** was not similar to that of **1** to Pb^{2+}, which confirmed the direct binding between Pb^{2+} and the carboxyl in **1**.

Comparison DGT with DGGT

We also investigated the tri-peptide probe, **2**, under the same conditions that we used for **1** to explore whether including another Gly in the probe would affect the recognition of metal ions. Probe **2** showed similar, but slightly different behaviors from **1** toward metal ions (Fig. S11–13†). The direct connection between the dansyl moiety and the tryptophan produced a probe, dansyl-L-Trp, which showed a modest blue-shift and quenching with the addition of Hg^{2+}, but no response with other metal ions [10]. Thus, the incorporation of either one or two Gly residues between the dansyl moiety and the Trp resulted in two tetra-functional dipeptide probes, **1** and **2**, which displayed distinct optical responses to Hg^{2+}, Cu^{2+}, Pb^{2+}, and H^{+} in aqueous solution. The different responses of **1**, **2**, and dansyl-L-Trp to Hg^{2+} reflected the different binding modes between them; thus, a peptide can provide more diversity in the binding site than a single amino acid. Despite the slight differences in fluorescence responses, both **1** and **2** interacted with Hg^{2+}, which suggested that a sulfonamide was necessary for the recognition of Hg^{2+}. This conclusion was further supported by the control molecules, **8** and **11**, which both had esterified moieties and also showed blue-shift or fluorescence enhancement in response to Hg^{2+} (Fig. S5†).

Cell Permeability of DGT and DGGT

Finally, we investigated the cell-permeability of **1** and **2** (Fig. 11). Cultured HEK-293 cells were incubated with 10 μM of **1** or **2** for 1 h at room temperature. The overlay of bright- field transmission and fluorescence images

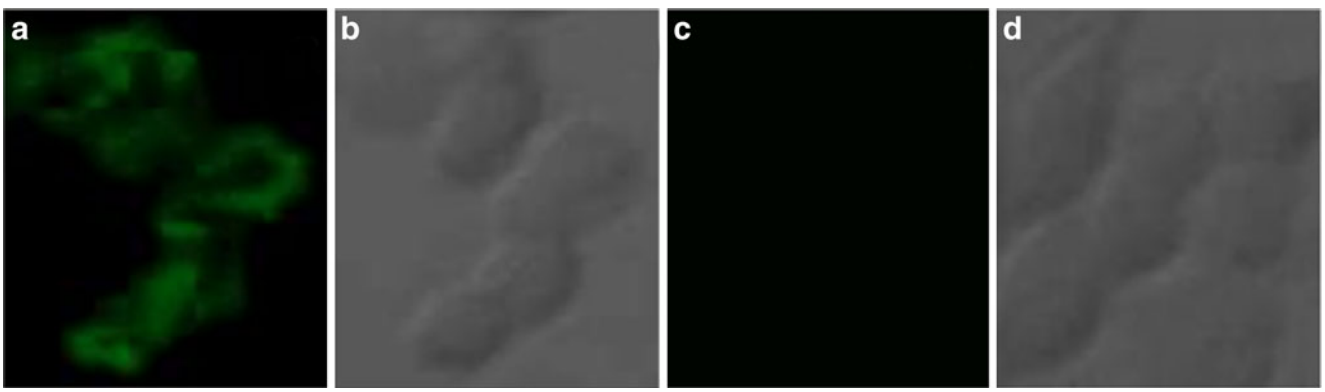

Fig. 11 Cell permeability of probes **1** and **2**. Confocal laser microscope images (**a**, **c**) and bright field images (**b**, **d**) of HEK-293 cells after incubating in the presence of **1** (**a**, **b**) and **2** (**c**, **d**). The difference in fluorescence brightness between **1** and **2** demonstrated that **1** showed more cell-permeability than **2**

revealed that **1** was localized in intracellular region, which demonstrated that **1** penetrated the cell membrane and accumulated inside the cell. Then we tried the fluorescence response of **1** to Hg^{2+} inside cell. However, as the inclusion of dansyl moiety of **1** in the hydrophobic cavity of BSA existed both in the cell and the culture medium induced the emission of **1** blue-shifted to the wavelength exactly as same as that of **1**/Hg^{2+}, the detection of Hg^{2+} in cell was interfered strongly [9]. In addition, the toxity of Hg^{2+} resulted in the cell readily to die for the long time incubation with Hg^{2+}. Therefore, we did not succeed. In contrast to **1**, **2** could not be detected in the intracellular region under the same conditions, which suggested that **2** was less cell permeable than **1**. This may due to the fact that **2** harbored an extra hydrophilic amino acid, glycine.

Conclusion

In summary, we synthesized a tetra-functional probe based on a dipeptide motif and a dansyl moiety, which responded to Hg^{2+} and Cu^{2+} in distinct modes and distinguishing optical properties. In addition, **1** was sensitive to pH ranging from 2.0 to 5.0 and precipitated in the presence of Pb^{2+} in neutral conditions. The concepts presented here will contribute to the future development of miniaturized molecular probes with multi-functions.

Acknowledgements The authors are grateful to the projects of the Natural Science Foundation of China (No. 20934002 and 20973073), the National Basic Research Program (2007CB808006), the Programs for New Century Excellent Talents in University (NCET) and the 111 Project (B06009).

References

1. McRae R, Bagchi P, Sumalekshmy S, Fahrni CJ (2009) In situ imaging of metals in cells and tissues. Chem Rev 109(10):4780–4827
2. Nolan EM, Lippard SJ (2008) Tools and tactics for the optical detectin of mercuric ion. Chem Rev 108(9):3443–3480
3. Que EL, Domaille DW, Chang CJ (2008) Metals in neurobiology: probing their chemistry and biology with molecular imaging. Chem Rev 108(5):1517–1549
4. Kou S, Lee HN, van Noort D, Swamy KMK, Kim SH, Soh JH, Lee K-M, Nam S-W, Yoon J, Park S (2008) Fluorescent molecular logic gates using microfluidic devices. Angew Chem Int Ed 47(5):872–876
5. Suresh M, Ghosh A, Das A (2008) A simple chemosensor for Hg^{2+} and Cu^{2+} that works as a molecular keypad lock. Chem Commun 23(33):3906–3908
6. Dhir A, Bhalla V, Kumar M (2008) Ratiometric sensing of Hg^{2+} based on the calix[4]arene of partial cone conformation possessing a dansyl moiety. Org Lett 10(21):4891–4894
7. Kaur N, Singh N, Cairns D, Callan JF (2009) A multifunctional tripodal fluorescent probe: "off-on" detection of sodium as well as two-input and molecular logic behavior. Org Lett 11(11):2229–2232
8. Ma L, Liu Y, Wu Y (2006) A tryptophan-containing fluoroionophore sensor with high sensitivity to and selectivity for lead ion in water. Chem Commun 21(25):2702–2704
9. Ma L, Li Y, Li L, Sun J, Tian C, Wu Y (2008) A protein-supported fluorescent reagent for the highly-sensivive and selective detection of mercuy ions in aqueous solution and live cells. Chem Commun 23(47):6345–6437
10. Li H-W, Li Y, Dang Y-Q, Ma L-J, Wu Y, Hou G, Wu L (2009) An easily prepared hypersensitive water-soluble fluorescent probe for mercury(II) ions. Chem Commun 24(29):4453–4455
11. Joshi BH, Park J, Lee WI, Lee KH (2009) Ratiometric and turn-on monitoring for heavy and transition metal ions in aqueous solution with a fluorescent peptide sensor. Talanta 78(3):903–909
12. Zheng Y, Leblanc RM (2002) A dansylated peptide for the selective detection of copper ions. Chem Commun 17(20):2350–2351
13. Berton M, Mancin F, Stocchero G, Tecilla P, Tonellato U (2001) Self-assembling in surfactant aggregates: an alternative way to the realization of fluorescence chemosensors for Cu(II) ions. Langmuir 17(24):7521–7528
14. Zheng Y, Leblanc RM (2003) Peptidyl fluorescent chemosensors for the detection of divalent copper. Anal Chem 75 (7):1706–1712
15. Frisch MJ, Trucks GW, Schlegel HB, Scuseria GE, Robb MA, Cheeseman JR, Scalmani G, Barone V, Mennucci B, Petersson GA, Nakatsuji H, Caricato M, Li X, Hratchian HP, Izmaylov AF, Bloino J, Zheng G, Sonnenberg JL, Hada M, Ehara M, Toyota K, Fukuda R, Hasegawa J, Ishida M, Nakajima T, Honda Y, Kitao O, Nakai H, Vreven T, Montgomery JA, Peralta JE Jr, Ogliaro F, Bearpark M, Heyd JJ, Brothers E, Kudin KN, Staroverov VN, Kobayashi R, Normand J, Raghavachari K, Rendell A, Burant JC, Iyengar SS, Tomasi J, Cossi M, Rega N, Millam JM, Klene M, Knox JE, Cross JB, Bakken V, Adamo C, Jaramillo J, Gomperts R, Stratmann RE, Yazyev O, Austin AJ, Cammi R, Pomelli C, Ochterski JW, Martin RL, Morokuma K, Zakrzewski VG, Voth GA, Salvador P, Dannenberg JJ, Dapprich S, Daniels AD, Farkas O, Foresman JB, Ortiz JV, Cioslowski J, Fox DJ (2009) Gaussian 09, Revision A. 02 Gaussian, Inc., Wallingford
16. Taki M, Desaki M, Ojida A, Iyoshi S, Hirayama T, Hamachi I, Yamamoto Y (2008) Fluorescnece imaging of intracellular cadmium using a dual-excitation rationmetric chemosensor. J Am Chem Soc 130(38):12564–12565
17. Metiver R, Leray I, Valeur B (2004) Photophysics of calixarenes bearing two or four dansyl fluorophores: charge, proton and energy transfers. Photochem Photobiol Sci 3(4):374–380
18. Chandrasekhar V, Bag P, Pandey MD (2009) Phosphorus-supported multidentate coumarin-containing fluorescence sensor for Cu^{2+}. Tetrahedron 65(47):9876–9883
19. Rurack K, Resch-Genger U (2002) Rigidization, preorientation and electronic decoupling- the 'magic triangle' for the design of highly efficient fluorescent sensors and switches. Chem Soc Rev 31(2):116–127
20. Bag B, Bharadwaj PK (2005) Perturbation of the PET process in fluorophore-spacer-receptor systems through structural modification: transition metal induced fluorescence enhancement and selectivity. J Phys Chem B 109(10):4377–4390
21. Bi X, Heng CH, Yang K-L (2008) A method of obtaining high selectivity for copper ions on triglycine decorated surfaces. J Phys Chem C 112(33):12887–12893
22. The U.S. Enviromental Protection Agency (EPA) has set the limit of copper in drinking water to be 1.3 ppm (~20 μM)
23. Wang J, Wang D, Miller EK, Moses D, Bazan GC and Heeger AJ (2000) Photoluminescence of water-soluble conjugated polymers: origin of enhanced quenching by charge transfer. Macromolecules 33(14):5153–5158
24. Deacon GB, Phillips RH (1980) Relationships between the carbon-oxygen stretching frequencies of carboxylate complexes

and the type of carboxylate coordination. Coord Chem Rev 33 (3):227–250
25. Nakamoto K (1986) Infrared and Raman spectra. Wiley, New York
26. Wold CR, Ni H, Soucek MK (2001) Model reaction study on the interaction between the inorganic and organic phases in drying oil based creamer coatings. Chem Mater 13(9):3032–3037
27. Ren Y, Iimura KI, Ogawa A, Kato T (2001) Surface micelles of CF3(CF2)(7)(CH2)(10)COOH on aqueous La3+ subphase investigated by atomic force microscopy and infrared spectroscopy. J Phys Chem B 105(19):4305–4312
28. Finnie KS, Bartlett JR, Woolfrey JL (1998) Vibrational spectroscopic study of the coordination of (2,2-'-bipyridyl-4,4'-dicarboxylic acid) ruthenium (II) complexes to the surface of nanocrystalline titania. Langmuir 14(10):2744–2749
29. Ma L-J, Li H-W, Wu Y (2009) A pyrene-containing fluorescent sensor with high selectivity for Lead (II) ion in water with dual illustration of ground-state dimer. Sens Actuators B 143(1):25–29